*actuators*

MDPI

*Article*

# Speed and Energy Efficiency of a Fish Robot Featuring Exponential Patterns of Control

**Ivan Tanev**

Graduate School of Science and Engineering, Doshisha University, Kyoto 610-0321, Japan; itanev@mail.doshisha.ac.jp

**Abstract:** Fish in nature have evolved more efficient swimming capabilities compared to that of propeller-driven autonomous underwater vehicles. Motivated by such knowledge, we discuss a bionic (bio-memetic) autonomous underwater vehicle—a fish robot—that mimics the swimming of rainbow trout (*Oncorhynchus mykiss*) in nature. The robot consists of three (anterior, posterior, and tail) segments, connected via two (anterior and posterior) actuated hinge joints. We divided the half-period of undulation of the robot into two phases—thrusting and braking. In addition, we hypothesized that an asymmetric duration—a short period of thrusting and a long period of braking—implemented as an exponential (rather than "canonical", sinusoidal) control would favorably affect the net propulsion of these two phases. The experimental results verified that, compared to sinusoidal undulation, the proposed exponential control results in increased speed of the robot between 1.1 to 4 times in the range of frequencies of undulation between 0.4 Hz and 2 Hz, and improved energy efficiency from 1.1 to 3.6 times in the same frequency range.

**Keywords:** bionic autonomous underwater vehicle; fish robot; asymmetric duration of phases of undulation; exponential control

## 1. Introduction

Fish in nature are known to have evolved an undulating swimming propulsion mechanism that is about two times more energy-efficient than that of autonomous underwater vehicles (AUVs) driven by screw propellers [1–3]. This inspired our research on AUVs that mimic the natural undulating propulsion of fish. Such bionic (biomimetic) AUVs (BAUVs) can potentially reach the same level of performance as their natural biological counterparts (e.g., fish) [4–9]. Moreover, BAUVs offer additional, significant advantages—that can favorably impact their applicability in eco-friendly monitoring, marine exploration, and the management of underwater living systems—such as weak wake, low noise, and lack of cavitation. However, optimization—at the level of control [4,10] or morphology [11–13] (or both)—of BAUVs might be needed before they reach the same level of performance and efficiency—tuned over millions of years of evolution—of their natural counterparts.

As a case study of BAUVs, in our research, we adopted an in-house-built fish robot (Fishbot) that models the natural rainbow trout (*Oncorhynchus mykiss*) [4]. Its swimming locomotion belongs to the group of the subcarangiform, in which the propulsion is mainly generated by the caudal fin and the posterior part of the body [14]. The bot consists of three (anterior, posterior, and tail) segments that are connected via two (anterior and posterior) actuated hinge joints. In our previous work, we heuristically optimized its main control parameters—the amplitude and frequency of undulation—via genetic algorithms (GAs) [4,15]. Also, we proposed an approach to solving the most significant challenge of

check for updates

Academic Editor: Gary M. Bone

Received: 27 January 2025
Revised: 24 February 2025
Accepted: 27 February 2025
Published: 28 February 2025

**Citation:** Tanev, I. Speed and Energy Efficiency of a Fish Robot Featuring Exponential Patterns of Control. *Actuators* **2025**, *14*, 119. https://doi.org/10.3390/act14030119

genetic algorithms (and evolutionary computing in general)—the significant runtime of the evolution of real, physical (rather than simulated) robots—by minimizing the runtime of the most time-consuming stage of evolution—the fitness trials [16]. In addition, we proposed a novel morphology for the robot—a limitedly underactuated posterior joint—and verified that, compared to its fully actuated implementation, such a morphology yields both a higher speed and better energy efficiency of the bot [13].

However, all of our previous efforts were focused on how to optimize the *morphology* of the robot. Conversely, in our current research, we intend to explore the possibility of improving the performance (e.g., speed and energy efficiency) of the bot by enhancing its *control* and specifically—by adopting an exponential pattern of control (i.e., the pattern of the target turning angles of servo motors and, consequently, the joints of the bot) actuators as an alternative to "canonical" sinusoidal control. Sinusoidal (harmonic) patterns have been commonly considered for the control of BAUVs because of their natural plausibility. Indeed, these patterns are a good approximation of the patterns observed in natural fish [17]. Moreover, such harmonic patterns result in low acceleration and low jerk of the movements of the joints, which, in turn, minimizes the wear-and-tear of the electro-mechanical components of the robot.

The inspiration for our current work is fueled by our assumption that during each half of the undulation cycle, the thrust is mainly generated by the movement of the posterior segment—the caudal (tail) fin—of the bot during the initial phase of undulation. In the remaining undulation, the fin is subjected to a hydrodynamic drag as it moves against the flow of the surrounding water. Based on such a decomposition of the undulation into thrusting- and braking phases, we hypothesize that an increased angular speed (and the corresponding linear speed of the tip of the posterior fin) would enhance the effect of the thrusting phase, while, at the same time, a reduced speed during the braking phase would diminish the negative effect of the latter.

An additional interest of this research stems from our observations that the downstroke (i.e., the thrusting phase of undulation) of some water creatures, such as the red-eared slider (*Trachemys scripta elegans*, Figure 1a) and the moon jellyfish (*Aurelia aurita*, Figure 1b), is quicker (i.e., shorter in time) than the upstroke—the braking phase of undulation. Despite the fact that we could not verify any asymmetry in the duration of the undulatory phases of natural fish, we were curious about the feasibility of adopting an analogy of such asymmetry, induced by the natural evolution, in the control of the Fishbot.

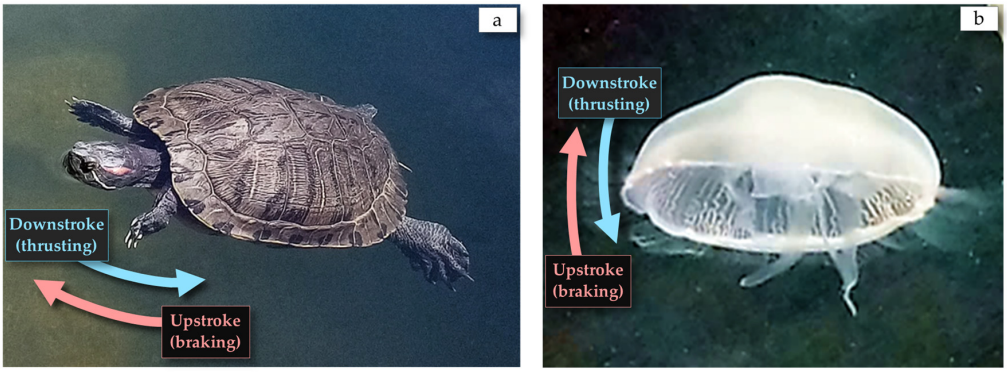


**Figure 1.** The downstroke—i.e., the thrusting phase of undulation—of both the red-eared slider *Trachemys scripta elegans* (**a**) and the moon jellyfish *Aurelia aurita* (**b**) is quicker (shorter in time) than the upstroke (braking). Photos by the author.

Our objective is to explore whether the exponential control—as a case of control that offers such a difference in the speed (and, consequently, asymmetry in duration) of thrusting and braking phases of undulation—would facilitate a higher net effect of the

two phases of undulation that could be manifested by an increased swimming speed or (and) better energy efficiency of the robot. To the best of our knowledge, we are not aware of any implementations of such exponential control of fish robots. As possible alternatives to sinusoidal undulations (Figure 2a), "square-like" (Figure 2b) and "triangular-like" (Figure 2c) motions have been previously considered [18]. None of these alternative, non-sinusoidal patterns of undulation, however, feature any time asymmetry of the main phases of undulation. Indeed, in both "square-like" and "triangular-like" undulations, the thrusting and braking phases of undulation (at least theoretically) have identical durations. Moreover, both the theoretical and experimental analysis of the advantages of these non-sinusoidal undulations do not necessarily require a decomposition of the undulation into distinct phases.

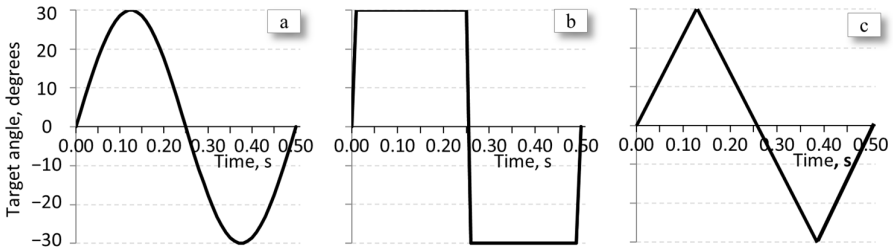


**Figure 2.** Sample sinusoidal—(**a**), square—(**b**), and triangular—(**c**) undulations. The frequency and amplitude of undulations of all three patterns are equal to 2 Hz and 30°, respectively.

The remainder of the paper is organized as follows. In the second section, we elaborate on the proposed concept of exponential control and why we believe that it should have a positive net effect on the speed and energy efficiency of the robot. In the same section, we introduce the experimental setup. In Section 3, we present the experimental results that verify the beneficial effect of the proposed exponential control of the speed and energy efficiency of the robot. In Section 4, we discuss some limitations of the proposed approach. Finally, in Section 5, we draw conclusions.

## 2. Materials and Methods

### *2.1. The Design and Control of the Fishbot*

We adopted an in-house built two-joint Fishbot that models the natural rainbow trout fish (*Oncorhynchus mykiss*) [4]. The bot comprises three (anterior, posterior, and tail) segments, connected via two (anterior and posterior) actuated hinge joints, as illustrated in Figure 3.

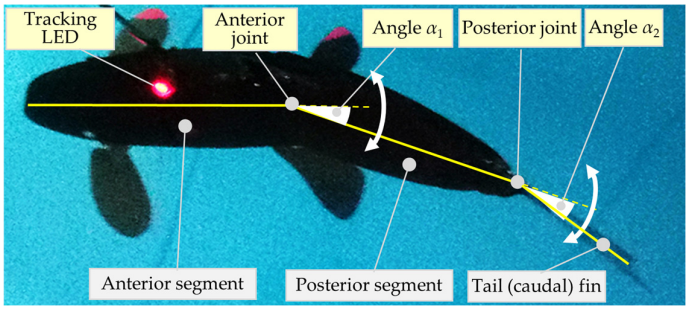


**Figure 3.** The Fishbot and its simplified kinematic diagram.

The two joints are undulated by two servo motors. Each motor is originally governed by a ("canonical") sinusoidal control signal (generated by the controller—the central pattern

generator) that sets the instant values of the angles $\alpha_1$ and $\alpha_2$ of the joints with a sampling interval of 20 ms, as expressed in the following Equations (1) and (2):

$$\alpha_1(t) = A_1 \times sin(2 \times \pi \times f \times t) \quad (1)$$

$$\alpha_2(t) = A_2 \times sin(2 \times \pi \times f \times t + \beta) \quad (2)$$

where $f$ is the frequency of undulation, $A_1$ is the angular amplitude of the anterior joint, $A_2$ is the angular amplitude of the posterior joint, and $\beta$ is the phase shift between the two signals, $\alpha_1$ and $\alpha_2$. Details on the design and control of the robot are elaborated in [4].

In our previous research on the bot, we used genetic algorithms to evolve the optimal values of the four main parameters of the sinusoidal control, $A_1$, $A_2$, $f$, and $\beta$, that yield the fastest speed of swimming [4,15,16]. In the current work, we used the evolved optimal values of these parameters, as well as the resulting speed of locomotion (and associated energy efficiency) of the bot featuring such sinusoidal control as a benchmark for comparison with the experimental results of the newly proposed (exponential) control.

### 2.2. Analysis of Undulation

The propulsion of the swimming Fishbot is generated by the undulations of the two actuated hinge joints. As illustrated in Figure 4, a single undulation can be split into the following two phases [19]: beginning (thrusting, Figure 4a), which could be seen as an analog to the downstroke of the red-eared slider and the moon jellyfish (Figure 1), and ending (braking, Figure 4c), similar to the upstroke as illustrated in Figure 1. The smooth transition between these two phases is manifested by a short intermediate phase, as shown in Figure 4b.

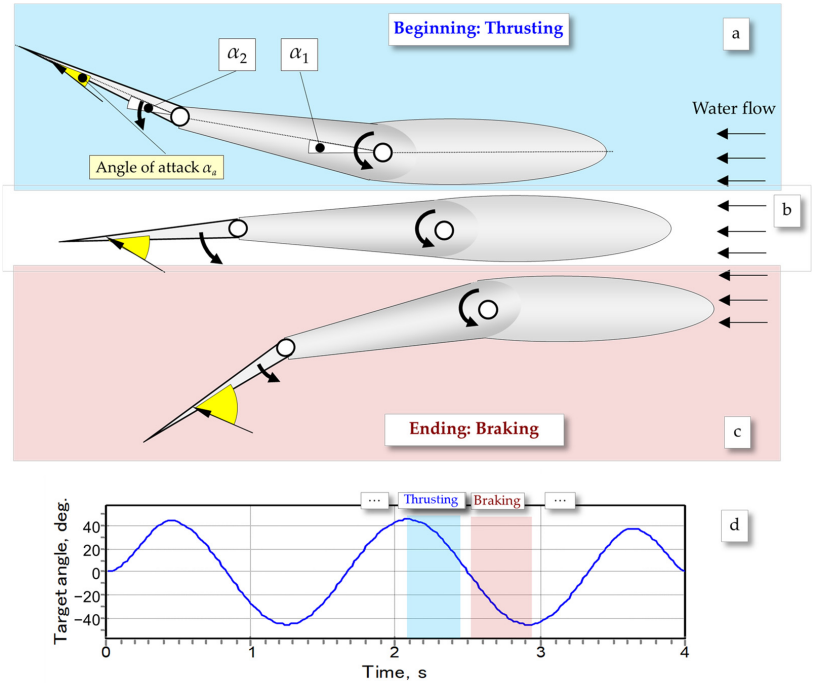


**Figure 4.** Phases of undulation of the Fishbot: (**a**) beginning (thrusting) and (**c**) ending (braking), with an intermediate (transition) phase between the two (**b**). The angles $\alpha_1$, $\alpha_2$, and $\alpha_a$ denote the deviation of the two joints and the angle of attack of the caudal fin, respectively. Note that the angle of attack is relatively small at the beginning of undulation and then gradually increases above values that exceed the critical value (typically, about 15°) by the end of undulation. The sample (sinusoidal) control signal of both actuators (**d**) corresponds to the following values of the main parameters of undulation: $A_1$ = 45°, $A_2$ = 45°, and $f$ = 0.6 Hz and the phase shift $\beta$ = 0°.

According to the dynamic lift theory of fish locomotion [20], at the beginning of undulation (Figure 4a), the moving caudal fin—due to the certain angle of attack—produces a lift (thrust) $L$ by pushing the water in the backward direction:

$$L = 0.5 \times C_L \times \rho \times U^2{}_T \times A \quad (3)$$

where $C_L$ is the coefficient of lift (thrust) of the fin, $\rho$ is the density of the fluid (water), $U_T$ is the average velocity of the fin, and $A$ is the planform area of the fin. Thus, the change in thrust impulse $\Delta P_T$ during the thrusting phase can be expressed as follows:

$$\Delta P_T = L \times T_T = 0.5 \times C_L \times \rho \times U^2{}_T \times A \times T_T \quad (4)$$

where $T_T$ is the duration of the thrusting phase of undulation. Considering that $U_T = l_T/T_T$, where $l_T$ is the distance the caudal fin travels during the thrusting phase, Equation (4) can be rewritten as follows:

$$\Delta P_T = 0.5 \times C_L \times \rho \times l^2{}_T \times A/T_T \quad (5)$$

For symmetrical hydrofoils, such as the caudal fin of fish, the coefficient of lift $C_L$ in the above Equation (5) can be approximated as follows:

$$C_L \approx 2 \times \pi \times \alpha_a \quad (6)$$

where $\alpha_a$ is the angle of attack of the fluid. However, the above Equation (6) holds only for small values (up to the critical value of about 15°) of $\alpha_a$, i.e., only during the first phase (beginning) of undulation (Figure 4a).

For values of $\alpha_a$ that are higher than the critical one, a stall of the fin occurs, which is manifested by the separation of the (turbulent) flow behind the fin. The stall results in an abrupt reduction in the lift (thrust) and a significant increase in the hydrodynamic drag. Starting from the intermittent phase of undulation (Figure 4b,c), in which the fin moves at a blunt angle relative to the water flow, the caudal fin stalls and is not able to produce any thrust. Moreover, as the caudal fin moves in the opposite direction to the water flow (Figure 4c), it is subjected to a high-pressure build-up at the front part of the fin (i.e., the "lower" part of the hydrofoil) and a low-pressure area in the rear part of the fin (the "upper" part of the hydrofoil). Such a pressure difference will result in turbulent fluid flow between the front and rear parts of the fin, resulting in flow separation and, ultimately, hydrodynamic pressure (form) drag $D$ that can be expressed as follows [21]:

$$D = 0.5 \times C_D \times \rho \times U^2{}_B \times A \quad (7)$$

where $C_D$ is the coefficient of drag, $\rho$ is the density of the fluid (water), $U_B$ is the average velocity of the fin, and $A$ is the planform area of the fin. The hydrodynamic drag $D$ would yield a detrimental braking effect and a corresponding change in the braking impulse $\Delta P_B$:

$$\Delta P_B = D \times T_B = 0.5 \times C_D \times \rho \times U^2{}_B \times A \times T_B \quad (8)$$

where $T_B$ is the duration of the thrusting phase of undulation. Because $U_B = l_B/T_B$, where $l_B$ is the distance the fin travels during the braking phase, Equation (8) can be rewritten as follows:

$$\Delta P_B = 0.5 \times C_D \times \rho \times l^2{}_B \times A/T_B \quad (9)$$

The overall propulsion force depends on the ratio of changes in the thrust and braking impulses—as expressed in Equations (5) and (9) in the above-mentioned two phases of

undulation [21,22]. Consequently, enhancing the thrust or (and) diminishing the braking associated with these phases of undulation might result in a favorable net increase in propulsion. We shall elaborate in the next subsection on how the proposed exponential control could achieve such an overall increase in thrust.

For simplicity, we assume that the water flow in the front part of the caudal fin is both (i) laminar and (ii) in a direction nearly parallel to the longitudinal axis of the anterior segment of the robot. In reality (e.g., due to the vortices, Coanda effect, etc.) this might not be exactly the case. Also, in Equation (7), we consider the pressure drag only, ignoring the second component of the overall drag—the skin friction drag. We assume that the latter is negligible due to the streamlined body of the Fishbot and its smooth fairings. Nevertheless, we believe that these assumptions do not compromise the fidelity of the proposed approach.

### *2.3. The Concept of the Exponential Control of the Fishbot*

The proposed approach assumes that, as mentioned above, the net propulsion of the Fishbot would depend on the ratio of the change in thrust and braking impulses (as expressed by Equations (5) and (9), respectively) during the corresponding two phases of undulation. Thus, we argue that maximizing this thrust-to-brake ratio of changes in impulses would result in an increase in the net propulsion of the robot. From Equations (5) and (9), we obtain this thrust-to-brake ratio $R_{TTB}$ as follows:

$$R_{TTB} = \Delta P_T / \Delta P_B = (C_L / C_D) \times ({l^2}_T / {l^2}_B) \times (T_B / T_T) \quad (10)$$

Assuming that $l_T \approx l_B$, the above Equation (10) could be rewritten as follows:

$$R_{TTB} = (C_L / C_D) \times (T_B / T_T) \quad (11)$$

As follows from the above Equation (11), a hypothetical control signal that maximizes the ratio $T_B/T_T$ would, in theory, result in a higher thrust-to-brake ratio $R_{TTB}$, that, in turn, would yield a higher speed and, presumably, better energy efficiency of the robot. Notice that, for the commonly adopted sinusoidal undulation, as expressed in Equations (1) and (2) and illustrated in Figure 2a, as well as the alternative "square-like" (Figure 2b) and "triangular-like" (Figure 2c) undulations, there is no such asymmetry in the duration of the two phases of undulation, $T_B$ and $T_T$. Consequently, the ratio $T_B/T_T$ is equal to 1 in these undulations.

In our quest for control of both actuators of the Fishbot, which would result in an increased ratio $T_B/T_T$, we shall consider a mathematical function that fulfills the following three intuitive criteria:

- While an increased ratio $T_B/T_T$ is sought, the sum $T_B + T_T$ should be equal to half of the period of undulation;
- An increased ratio $T_B/T_T$ implies that the average derivative (i.e., gradient) of the function of the target turning angle of servo motors during the thrusting phase should be higher than that of the braking phase;
- The transition between the two (thrusting and braking) phases should be smooth, with the higher instant derivative of the function of the target turning angle of servo motors during the thrusting phase gradually approaching the lower values pertinent to the braking phase of undulation;
- The target turning angle of servo motors of both phases of undulation should (preferably) be expressed by the same (monotonous) function.

We propose an exponential function of control, as shown in Figure 5, because it fulfills the above-mentioned criteria. The proposed exponential control signal can be analytically expressed as follows:

$$\alpha = -A_{SM} + (A_{SM} + A_{PS}) \times (1 - e^{-t/\tau}) \quad (12)$$

where $\alpha$ is the instant value of the turning angle of (either anterior or posterior) servo motors, $A_{SM}$ is the amplitude of undulation (i.e., the maximum value of the turning angle of the servo motor), $A_{PS}$ is the amplitude of the imaginary pulse signal that defines the asymptotic value of $\alpha$, $t$ is the time, and $\tau$ is a time constant (Figure 6).

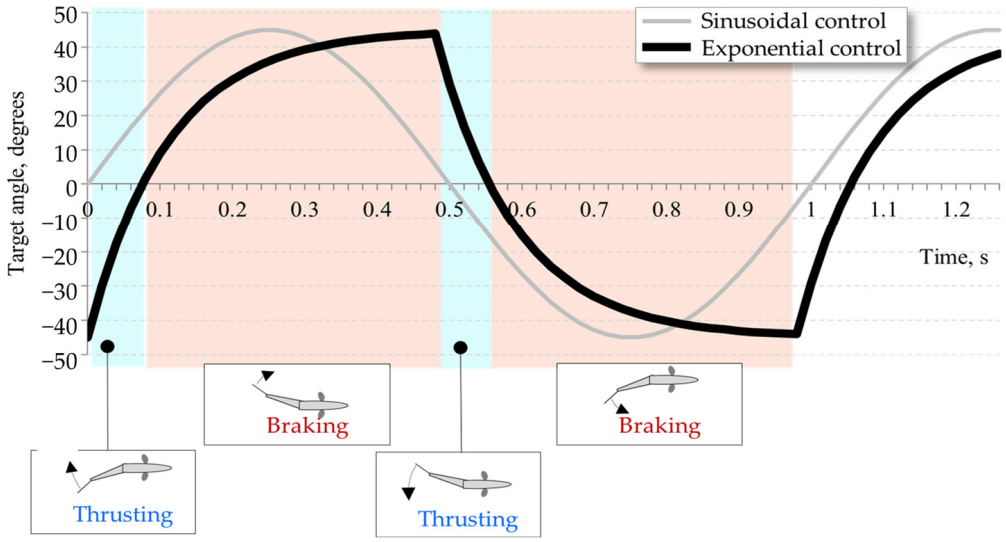


**Figure 5.** The concept of the exponential control of the servo motors that, compared to the sinusoidal control, features an increased ratio of the durations of the braking and thrusting phases of undulation.

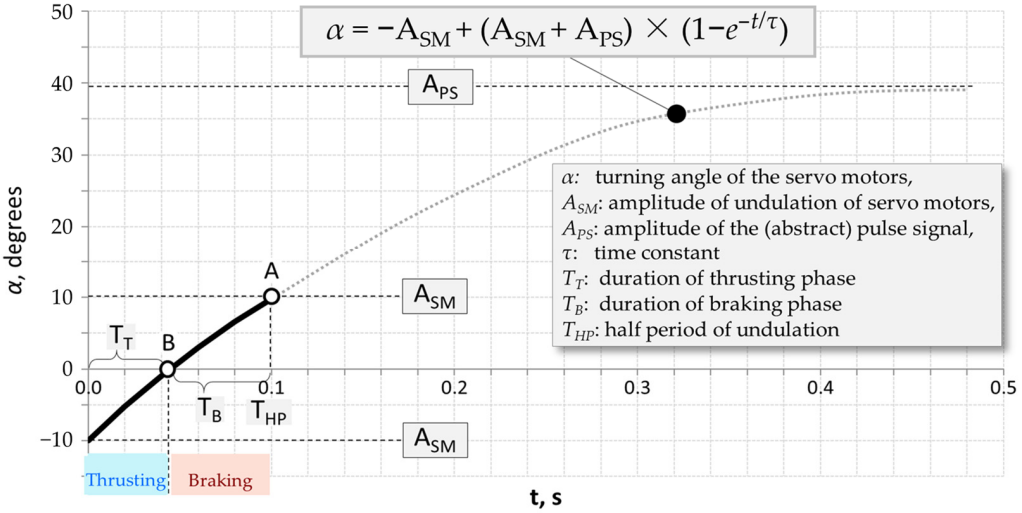


**Figure 6.** The main parameters of the proposed exponential function of control of the Fishbot.

In order to investigate the effect of the ratio $T_B/T_T$ on the speed and energy efficiency of the bot, for a given frequency (and corresponding duration of the half-period $T_{HP}$) and amplitude $A_{SM}$ of undulation, we would need to define the two main parameters—$A_{PS}$ and $\tau$, respectively—of the exponential function, as expressed in Equation (12). We can define these two unknown parameters from the following system of two Equations (13) and (14).

These two equations express the value of the exponential function at the points of time A and B, respectively, as shown in Figure 6:

$$\alpha = -A_{SM} + (A_{SM} + A_{PS}) \times \left(1 - e^{-T_{HP}/\tau}\right) = A_{SM} \quad (13)$$

$$\alpha = -A_{SM} + (A_{SM} + A_{PS}) \times (1 - e^{-T_{HP}/((R+1)\times\tau)}) = 0 \quad (14)$$

where $R = T_B/T_T$. The analytically obtained solution of the above system can be expressed in a general form as follows:

$$\mathrm{A_{PS}} = \mathrm{k_{ps}} \times \mathrm{A_{SM}} \quad (15)$$

$$\tau = k_\tau \times T_{HP} \quad (16)$$

Consequently, Equation (12) can be rewritten as follows:

$$\alpha = -A_{SM} + \left(A_{SM} + k_{ps} \times A_{SM}\right) \times \left(1 - e^{-t/(k_\tau \times T_{HP})}\right) \quad (17)$$

The concrete analytical solutions—the obtained values of the coefficients $k_{ps}$ and $k_\tau$—that define the values of parameters $A_{PS}$ and $\tau$, respectively, of the exponential function are shown in Table 1 for different values of the ratio $T_B/T_T$.

**Table 1.** Values of coefficients $k_{ps}$ and $k_\tau$ defining the main parameters $A_{PS}$ and $\tau$ of the exponential control of the Fishbot for various ratios of $R = T_B/T_T$.

| $\boldsymbol{R = T_B/T_T}$ | $\boldsymbol{k_{ps}(A_{PS} = k_{ps} \times A_{SM})}$ | $\boldsymbol{k_\tau(\tau = k_\tau \times T_{HP})}$ |
|---|---|---|
| 2 | 1.618 | 0.693 |
| 3 | 1.192 | 0.410 |
| 4 | 1.078 | 0.305 |
| 6 | 1.017 | 0.209 |
| 8 | 1.004 | 0.161 |
| 10 | 1.001 | 0.131 |

Consequently, for example, for $R = T_B/T_T = 2$, the control of the servo motors for a given amplitude ($A_{SM}$) and half period ($T_{HP}$) of undulation would be defined by the following Equation (18):

$$\alpha = -A_{SM} + (A_{SM} + 1.618 \times A_{SM}) \times \left(1 - e^{-t/(0.693\times T_{HP})}\right) \quad (18)$$

Analogically, for example, for the ultimate value of $R = T_B/T_T = 10$, the control of the servo motors would be expressed as follows:

$$\alpha = -A_{SM} + (A_{SM} + 1.001 \times A_{SM}) \times \left(1 - e^{-t/(0.132\times T_{HP})}\right) \quad (19)$$

The forms of the control signals, defined by the obtained values of the main parameters of the exponential control of undulation $A_{PS}$ and $\tau$ for $A_{SM} = 45^\circ$, $T_{HP} = 0.25$ s ($f = 2$ Hz), and different values of the ratio $R = T_B/T_T$ are shown in Figure 7.

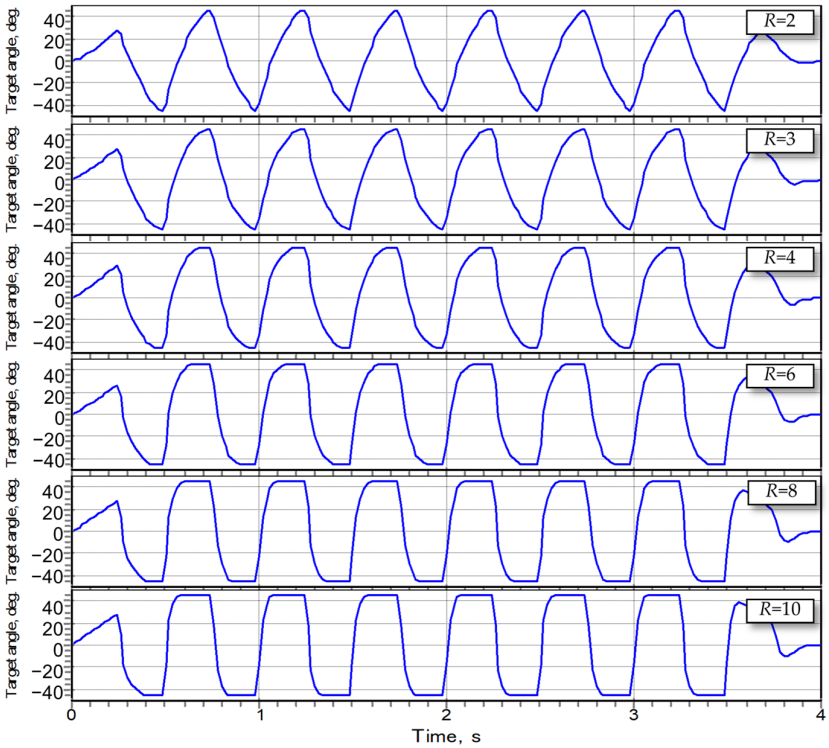


**Figure 7.** The exponential control signals $\alpha$ (i.e., the target angle of the two servo motors, with no phase shift between them), defined by the obtained values of the main parameters of the exponential control of undulation $A_{PS}$ and $\tau$ for $A_{SM}$ = 45°, $T_{HP}$ = 0.25 s ($f$ = 2 Hz), and different values of the ratio $R = T_B/T_T$.

## 3. Experimental Results

### *3.1. Experimental Setup*

To investigate the effect of the proposed exponential control—in which the instant values of turning angles of both servo motors of the Fishbot are set according to Equation (17)—on both the speed of locomotion and energy efficiency of the bot, we conducted experiments with six different values of the ratio $R = T_B/T_T$, equal to 2, 3, 4, 6, 8, and 10. For each value of this ratio, we ran four trials (to account for the effect of environmental noise) of the bot with a given frequency of undulation $f$ (i.e., a given half-period of undulation—the parameter $T_{HP}$ in Equation (17)), with the maximum amplitude of undulation of both servo motors (i.e., parameter $A_{SM}$ in Equation (17) set to 45°), and no phase shift between the exponential signals of the two servo motors. Our decision to run just four trials is based on the preliminary investigation of the consistency of the results obtained from each trial. The maximum value of the standard deviation of the speed and energy efficiency is just about 2% of the experimentally obtained values—much lower compared to the differences in speed and energy efficiency due to the proposed exponential control of the robot.

We verified in our previous research that the maximum amplitude of undulation does indeed result in maximum speed and energy efficiency of the bot [4,15,16]. We tested five different frequencies $f$ ranging from 0.4 Hz ($T_{HP}$ = 1.25 s) to 2.0 Hz ($T_{HP}$ = 0.25 s) with a discretization step of 0.4 Hz. The results of the four runs are aggregated based on the calculated mean of the achieved performance (e.g., speed and energy efficiency).

The experimental system consists of the Fishbot, its controller, and an optical tracker, as depicted in Figure 8. The controller consists of an abstract layer and a physical layer. The former generates the exponential control signals—the instant values of the turning angles of servo motors, as of Equation (17)—with a sampling interval of 20 ms. The physical layer converts the values of the turning angles of servo motors, generated by the abstract layer

into pulse-width modulated signals that physically govern the instant angular positions of the servos. In addition, in order to measure the electrical power consumed by the robot during the trials, we connected a current sensor serially to the power supply ($Ucc$ = 5 V) line of the robot. We adopted the Micro Maestro 6-Channel USB Servo Controller and ACS724—both produced by Pololu Robotics and Electronics [23,24]—as a hardware implementation of the physical layer and the current sensor, respectively.

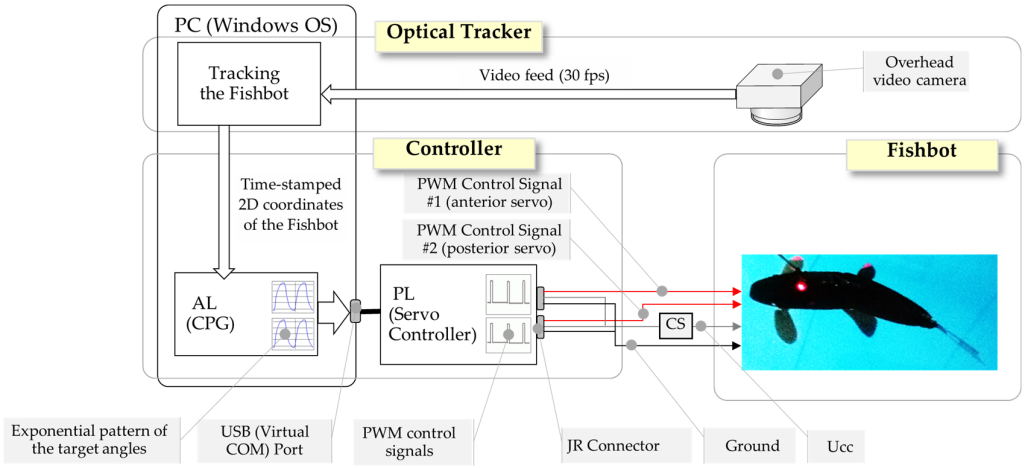


**Figure 8.** The structure of the experimental system. The abbreviations AL, CPG, PL, PWM, and CS denote the abstract layer, central pattern generator, physical layer, pulse-width modulation, and current sensor, respectively.

In addition to the Fishbot and its controller, the experimental system also includes an optical tracker, which uses a video feed from an overhead video camera to track (via a bright red LED mounted on the bot, as shown in Figure 3) the timestamped 2D positions of the swimming Fishbot. From the timestamped 2D coordinates of the bot, obtained from the optical tracker, the controller estimates the instant speed of the bot during the 5 s swimming trial. The maximum value of the instant speed is assumed to be the actual steady-state swimming speed of the Fishbot. Also, based on the readings from the current sensor (denoted as CS in Figure 8), and the speed of the bot, the controller calculates the energy efficiency of the latter, as elaborated below in Section 3.3. The third version of the software of the abstract layer of the controller, and the optical tracker, both developed by the author, was used. The details of the experimental setup are elaborated in [3,13,16].

### *3.2. Swimming Speed*

Figure 9 illustrates the experimentally obtained speed of locomotion as a function of the frequency of oscillations $f$ and the value of the ratio $R = T_B/T_T$. As shown in Figure 9a, for frequencies up to $f$ = 1.6 Hz, the increase in the ratio $R = T_B/T_T$ results in an increase in the swimming speed of the robot. The maximum speed-up of four times, compared to the canonical sinusoidal control, is achieved for $R$ = 10 and $f$ = 0.4 Hz. With the increase in the frequency of undulation, however, the favorable effect of the exponential control gradually decreases, and, moreover, at the maximum frequency of 2 Hz, the fastest speed is achieved for $R$ = 8 (Figure 9a), with a corresponding drop in the speed-up (compared to the sinusoidal control featuring the same main parameters of oscillation, such as amplitude, frequency, and no phase shift between the signals of the two servo motors) to about 1.15 times. Nevertheless, virtually for all frequencies of undulation, and all values of the ratio $R$ (with the only exception of $R$ = 2 for frequencies $f$ = 1.6 Hz and $f$ = 2 Hz), the exponential control is superior to that of the sinusoidal one in that it yields a faster robot swimming speed.

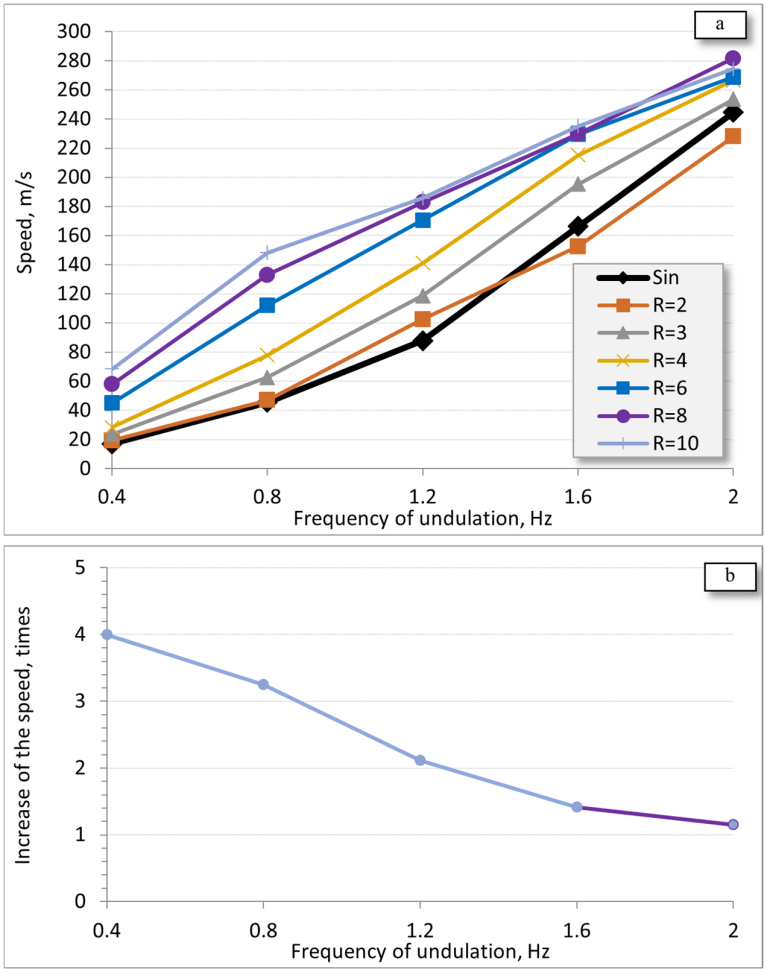


**Figure 9.** Maximum speed of the Fishbot as a function of the frequency of oscillations $f$ for different values of $R = T_B/T_T$ (**a**) and the increase in the swimming speed relative to the sinusoidal control (**b**).

### *3.3. Energy Efficiency*

The energy efficiency $E_E$ is estimated as the distance $D$ the Fishbot can swim autonomously with a given energy (e.g., stored in its batteries) $E_B$:

$$E_E = D/E_B \tag{20}$$

The above Equation (20) could be rewritten as follows:

$$E_E = (V \times T)/(I_{AVR} \times U_{CC} \times T) \tag{21}$$

and

$$E_E = V/(I_{AVR} \times U_{CC}) \tag{22}$$

where $T$ is the time the bot would eventually travel before it exhausts its available energy, $V$ is the swimming speed, $I_{AVR}$ is the average electrical current consumed by the bot during the trial, and *Ucc* is the constant power supply voltage (5 V), respectively. We estimated the energy efficiency according to the above Equation (22).

As shown in Figure 10, compared to the sinusoidal control, the proposed exponential one results in improved (experimentally obtained) energy efficiency.

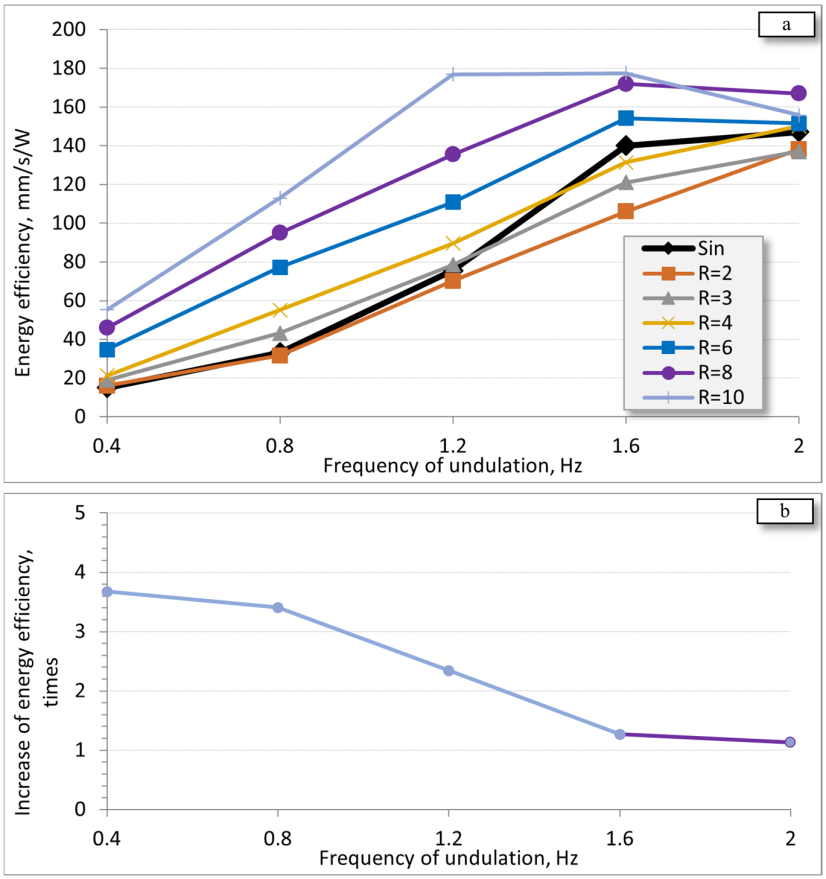


**Figure 10.** Energy efficiency of the Fishbot (**a**) and the increase in energy efficiency relative to the sinusoidal control (**b**).

Virtually for all frequencies $f$, the increase in the ratio $R = T_B/T_T$ yields better energy efficiency, with the only exception observed for the maximum frequency $f$ = 2 Hz, and the maximum value of $R$ = 10. Compared to the canonical sinusoidal control, the maximum increase in energy efficiency of about 3.7 times is achieved for $R$ = 10 and $f$ = 0.4 Hz (Figure 9a,b). The maximum absolute value of the energy efficiency of about 177 mm/s/W is achieved for $R$ = 10 and a frequency between 1.2 Hz and 1.6 Hz (Figure 9a). With the increase in the frequency of undulation, however, the energy efficiency of the exponential control gradually decreases; moreover, the exponential control with lower values of $R$ is even less energy efficient than that of the sinusoidal one.

## 4. Discussion

Compared to the sinusoidal control, the proposed exponential control yields improved performance (e.g., swimming speed and energy efficiency) of the Fishbot. However, the favorable effect of the control somehow diminishes at higher frequencies of undulation. We argue that there are two possible causes for this: (i) the flexibility of the caudal fin and (ii) exceeding the technical specifications of the servo motors. Regarding the former cause, being subjected to excessive forces during the thrusting phase of the high-frequency undulations, the fin flexes too much, which, in turn, reduces the angle of attack $\alpha_a$ which—according to Equation (6)—results in a corresponding reduction in the coefficient of lift (thrust) of the fin. Therefore, in the future, it would be interesting to repeat our experiments with a stiffer robot caudal fin.

As for the latter cause—exceeding the technical specifications of the servo motors as a result of the more demanding exponential control—it is important to stress that the controller of the bot—according to Equation (17)—sets the instant values of the *desired*

(*target*) turning angles of servo motors rather than the *actual* one. Typically, the servo motors lack the capability to provide any feedback to the controller about the instant values of their actual turning angles. However, as a result of the interplay between (i) the dynamics of the desired turning angle, (ii) the extent of the external forces exerted on the moving segments of the bot, and (iii) the capabilities of the motor (according to its technical specifications) and, especially the maximum torque exerted by the servo and the maximum angular speed, the instant value of the *actual* turning angle of the motor may intermittently differ from the value of the *desired* one. This, in turn, would distort the actual control signal, as its rate of change would be lower than that of the desired one. The maximum angular speed (i.e., the rate limit) of the servo motors, used to build the Fishbot, is 600°/s [25], which, as depicted in Figure 11, for the frequency of undulation $f$ = 2 Hz, is exceeded by the desired angular speed. The latter is calculated as a derivative of the desired turning angle of the servo motors (as illustrated in Figure 7). As shown by the shaded areas in Figure 10, the peaks of the desired angular speed at the very onset of the thrusting phase of undulation intermittently exceed the speed limit of the servo motors (i.e., 600°/s) for the ratios $R = T_B/T_T$ equal to 4, 6, 8, and 10. Moreover, the increase in the value of $R$ results in an increase in both (i) the difference between the desired and actual (presumably, 600°/s) angular speeds and (ii) the duration during which the desired speed exceeds the actual one. Therefore, the increase in the ratio $R$, especially in high-frequency undulations, would result in increased severity of distortion of the intended exponential control signals. In our future research, it will be important to conduct additional experiments with an increased rate limit of the servo motors. One possible approach to achieving this would be simply raising the DC voltage of the power supply of the servo from the currently set *Ucc* = 5 V.

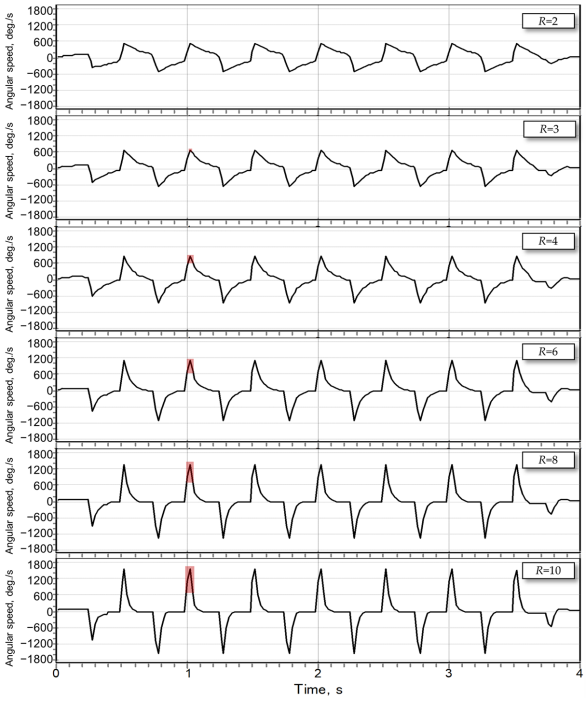


**Figure 11.** The angular speeds of the target angle of servo motors for $A_{SM}$ = 45°, $T_{HP}$ = 0.25 s ($f$ = 2 Hz), and different values of the ratio $R = T_B/T_T$. These speeds are obtained as derivatives of the time series of the instant values of the desired turning angles of the servo motors, as illustrated in Figure 7. As illustrated by the red shaded areas at around 1 s into the trial, the increase in the value of $R$ results in the increase in both (i) the difference between the desired and actual (600°/s) angular speeds and (ii) the duration during which the desired speed exceeds the actual one.

The potential real-world applications of the proposed exponential control could be in the energy-efficient monitoring and management of underwater living systems. Faster speed of locomotion might also favorably impact the range of the bot in upstream underwater currents. There are remaining challenges—such as navigation, communication, collecting and transmitting sensory information, and limited payload—that have to be addressed before the widespread adoption of BAUVs.

## 5. Conclusions

We decomposed the undulation of the Fishbot into two phases—thrusting and braking—and proposed an alternative—exponential (rather than sinusoidal)—pattern of control. The proposed control features an asymmetric duration of these two phases of undulation—shorter (faster) thrusting and longer (slower) braking. The experimental results suggest that, compared to bots featuring a sinusoidal undulation, the proposed exponential control favorably impacts the net effect of these two phases. Compared to the sinusoidal control (featuring identical values of the main parameters of oscillation, such as amplitude, frequency, and no phase shift between the signals of the two servo motors), the proposed exponential control yields between 1.1 and 4-times faster speeds in the range of frequencies of undulation between 0.4 Hz and 2 Hz and between 1.1 and 3.6 times higher energy efficiency in the same frequency range.

In our future work, we plan to address the challenge of the diminishing effect of the proposed exponential control at higher frequencies of undulation. In particular, we are interested in whether a stiffer caudal fin would be more responsive at the onset of the thrusting phase when the external forces exerted on the fin are highest. Also, we would like to consider increasing the angular speed limits of the servo motors in order to minimize the possible distortion of the intended exponential control signals caused by intermittently exceeding these limits during the high-speed undulations.

**Funding:** This research received no external funding.

**Data Availability Statement:** Data available upon a request to the author.

**Conflicts of Interest:** The author declares no conflicts of interest.

## References

1. Breder, C.M.; Breder, C.M. The locomotion of fishes. *Zool. Sci. Contrib. N. Y. Zool. Soc.* **1926**, *4*, 159–297. [CrossRef]
2. Fish, F. Swimming Strategies for Energy Economy. In *Fish Locomotion*; Eco-Ethological Perspect; CRC Press: Boca Raton, FL, USA, 2010. [CrossRef]
3. Mannam, N.P.B.; Alam, M.M.; Krishnankutty, P. Review of biomimetic flexible flapping foil propulsion systems on different planetary bodies. *Results Eng.* **2020**, *8*, 100183. [CrossRef]
4. Tanev, I. Fish Robot: Design, Control and Evolution of Undulatory Swimming Gaits. Technical Report, 2021; 33p. Available online: http://isd-si.doshisha.ac.jp/itanev/TR/TR_20210716_Fishbot.pdf (accessed on 24 December 2024).
5. Vo, T.Q.; Kim, H.S.; Lee, B.R. Smooth gait optimization of a fish robot using the genetic-hill climbing algorithm. *Robotica* **2012**, *30*, 257–278. [CrossRef]
6. Roper, D. Energy Based Control System Designs for Underactuated Robot Fish Propulsion. Ph.D. Thesis, University of Plymouth, Plymouth, UK, 2013. [CrossRef]
7. Wang, W.; Guo, J.; Wang, Z.; Xie, G. Neural controller for swimming modes and gait transition on an ostraciiform fish robot. In Proceedings of the 2013 IEEE/ASME International Conference on Advanced Intelligent Mechatronics, Wollongong, NSW, Australia, 9–12 July 2013; pp. 1564–1569. [CrossRef]
8. Wang, W.; Gu, D.; Xie, G. Autonomous Optimization of Swimming Gait in a Fish Robot with Multiple Onboard Sensors. *IEEE Trans. Syst. Man Cybern. Syst.* **2019**, *49*, 891–903. [CrossRef]
9. Zhu, J.; White, C.; Wainwright, D.K.; Di Santo, V.; Lauder, G.V.; Bart-Smith, H. Tuna robotics: A high-frequency experimental platform exploring the performance space of swimming fishes. *Sci. Robot.* **2019**, *4*, eaax4615. [CrossRef] [PubMed]

10. Iida, F.; Pfeifer, R.; Seyfarth, A. AI in Locomotion: Challenges and Perspectives of Underactuated Robots. In *50 Years of Artificial Intelligence: Essays Dedicated to the 50th Anniversary of Artificial Intelligence*; Lungarella, M., Iida, F., Bongard, J., Pfeifer, R., Eds.; Lecture Notes in Computer Science; Springer: Berlin, Heidelberg, 2007; pp. 134–143. [CrossRef]
11. Romano, D.; Wahi, A.; Miraglia, M.; Stefanini, C. Development of a Novel Underactuated Robotic Fish with Magnetic Transmission System. *Machines* **2022**, *10*, 755. [CrossRef]
12. Takada, Y.; Nakanishi, Y.; Araki, R.; Nonogaki, M.; Wakisaka, T. Effect of Material and Thickness about Tail Fins on Propulsive Performance of a Small Fish Robot. *J. Aero Aqua Bio-Mech.* **2010**, *1*, 51–56. [CrossRef]
13. Heinen, Y.; Tanev, I.; Kimura, T. The Effect of a Limited Underactuated Posterior Joint on the Speed and Energy Efficiency of a Fish Robot. *Appl. Sci.* **2024**, *14*, 5010. [CrossRef]
14. Di Santo, V.; Goerig, E.; Wainwright, D.K.; Lauder, G.V. Convergence of undulatory swimming kinematics across a diversity of fishes. *Proc. Natl. Acad. Sci. USA* **2021**, *118*, e2113206118. [CrossRef] [PubMed]
15. Komoto, T.; Tanev, I.; Shimohara, K. Evolving the Thrust of Undulatory Swimming Gaits of Fish Robot. In Proceedings of the 27th Symposium on Artificial Life and Robotics (AROB-ISBC-SWARM 2022), Beppu, Japan, 25 January 2022; p. 6.
16. Sancho, M.A.; Tanev, I.; Shimohara, K. Fitness Lookup Table Reduces the Runtime of Evolution of Swimming Gaits of Fish Robot. In Proceedings of the 28th Symposium on Artificial Life and Robotics (AROB-ISBC-SWARM 2023), Beppu, Japan, 25 January 2023; p. 6.
17. Čech, M.; Jarolím, O.; Kubecka, J.; Vašek, M.; Peterka, J.; Matěna, J. Sinusoidal swimming in fishes: Using hydroacoustics, underwater camera and direct sampling techniques to understand peculiar fish behavior. In Proceedings of the Modern Problems of Aquatic Ecology—4th International Scientific Conference to Commemorate Prof. G.G. Winberg, St. Petersburg, Russia, 11–15 October 2010. [CrossRef]
18. Van Buren, T.; Floryan, D.; Quinn, D.; Smits, A. Nonsinusoidal gaits for unsteady propulsion. *Phys. Rev. Fluids* **2017**, *2*, 053101. [CrossRef]
19. Bale, R.; Shirgaonkar, A.A.; Neveln, I.D.; Bhalla, A.P.S.; MacIver, M.A.; Patankar, N.A. Separability of Drag and Thrust in Undulatory Animals and Machines. *Sci. Rep.* **2014**, *4*, 7329. [CrossRef] [PubMed]
20. MacDonald, J. What Makes Fish Swim Fast. *JSTOR: Digital Library for Scholars, Researchers, and Students, October 3, 2017*. Available online: https://daily.jstor.org/what-makes-fish-swim-fast/ (accessed on 23 December 2024).
21. Arakeri, J.H. Fluid Mechanics of Fish Swimming: Lift-based Propulsion. *Resonance* **2009**, *14*, 32–46. Available online: https://www.ias.ac.in/article/fulltext/reso/014/01/0032-0046 (accessed on 24 December 2024). [CrossRef]
22. Webb, P.W. Simple Physical Principles and Vertebrate Aquatic Locomotion. *Am. Zool.* **1988**, *28*, 709–725. [CrossRef]
23. Pololu Robotics and Electronics. Micro Maestro 6-Channel USB Servo Controller. Available online: https://www.pololu.com/product/1350 (accessed on 23 December 2024).
24. Pololu Robotics and Electronics. ACS724LLCTR-2P5AB Current Sensor Carrier. Available online: https://www.pololu.com/product/4040 (accessed on 23 December 2024).
25. Huizhou AGF-RC Electronic Technology Company, A20CLS Programmable Micro Servo. Available online: https://www.agfrc.com/index.php?id=2429 (accessed on 26 January 2025).